Signatures of quantum integrability and exactly solvable dynamics in an infinite-range many-body Floquet spin system

Harshit Sharma [*] and Udaysinh T. Bhosale [†]
Department of Physics, Visvesvaraya National Institute of Technology, Nagpur 440010, India

(Received 10 May 2024; accepted 24 July 2024; published 14 August 2024)

In a recent work [Sharma and Bhosale, Phys. Rev. B **109**, 014412 (2024)], an N-spin Floquet model with infinite-range Ising interaction was introduced. In this paper, we generalize the strength of interaction to J, such that the $J = 1$ case reduces to the aforementioned work. We show that for $J = 1/2$ the model still exhibits integrability only for an even number of qubits. We analytically solve the cases of 6, 8, 10, and 12 qubits, finding the eigensystem, the dynamics of the entanglement for various initial states, and the unitary evolution operator. These quantities exhibit the signature of quantum integrability (QI). For the general case of even $N > 12$ qubits, we conjuncture the presence of QI using numerical evidence such as spectrum degeneracy and the exact periodic nature of both the entanglement dynamics and the time-evolved unitary operator. We numerically show the absence of QI for odd N by observing a violation of the signatures of QI. We analytically and numerically find that the maximum value of time-evolved concurrence ($C_{\max}$) decreases with N, indicating the multipartite nature of entanglement. Possible experiments to verify our results are discussed.

DOI: 10.1103/PhysRevB.110.064313

I. INTRODUCTION

Long-range interactions are encountered in various scientific domains, including statistical physics [1–3], quantum mechanics [4,5], cosmology [6–9], atomic and nuclear physics [10], plasma physics [11], hydrodynamics [12–14], and condensed matter physics [15]. This interaction can now be replicated in a quantum simulator [16–18] with artificial ion crystals [19–21], cold atoms in cavities [22], polar molecules [23], dipolar quantum gases [24–26], Rydberg atoms [27], magnetic atoms [28–30], nonlinear optical media [31], and solid-state defects [32]. It is also present between genomic elements which can be detected by using the chromosome conformation capture method [33] and in adatoms of graphene [34]. Long-range interactions are pervasive and give rise to qualitatively new physics, e.g., the emergence of novel quantum phase and dynamical behaviors [35,36]. Additionally, they play a crucial role in enabling speedup in quantum information processing [37,38]. Long-range interactions have been proven to be very useful in quantum technology applications like the quantum heat engine [39], quantum computing [40,41], quantum metrology [42], and ion traps [43].

Entanglement stands out as perhaps the most distinctive feature of quantum mechanics, giving rise to unique nonlocal correlations that find no counterpart in the classical domain. Long-range interactions have the potential to profoundly influence the dynamics of correlated systems [1]. Due to the breakdown of quasilocality in long-range interaction various phenomena arise such as its faster entanglement generation [38,44,45] than the Lieb-Robinson bound [46] and dynamical phase transitions [47,48]. Numerous studies have delved into the examination of entanglement in such systems [49–57]. The time evolution of multipartite entanglement measured using quantum Fisher information (QFI) and scrambling in a spin chain has been studied with these interactions [58]. They have been measured in experiments too [59].

The long-range interaction decays with distance r according to a power law ($1/r^{\alpha}$). Corresponding to different values of α, these interactions in the natural system fall into categories such as Rydberg atoms ($\alpha = 6$, van der Waals interactions), magnetic atoms ($\alpha = 3$, dipole- dipole interaction), Coulomb interactions ($\alpha = 1$), atoms coupled to cavities ($\alpha = 0$), etc. The case $\alpha = 0$ corresponds to a category of infinite-range or all-to-all interactions [23,60–71]. Models with $\alpha < d$ are categorized as long-range interaction, where d is the physical dimension of the system [1,15]. In such interactions, the energy is not extensive [1,3,15]. There are models corresponding to infinite-range interaction that are integrable, such as the Lipkin-Meshkov-Glick (LMG) model [72] and the model with Ising interaction in a transverse field [73]. The main theme of this paper revolves around integrability in one such recently introduced model [73].

From the perspective of classical mechanics, integrability can be understood by the connection between the degree of freedom and a sufficient number of constants of motion [74,75], whereas the quantum integrability [76–81] is typically associated with an exact solution of models, for example, based on the solution of the Yang-Baxter equation found by obtaining the transfer matrix [77,82–86], and techniques like the Bethe ansatz [87–90]. Alternatively, it can be identified through other features, for instance, the existence of a set of an infinite number of conserved quantities and/or Poissonian-level statistics after taking conserved quantities into account [91,92]. In various studies, the indication of integrability in

[*]Contact author: ds21phy007@students.vnit.ac.in
[†]Contact author: udaysinhbhosale@phy.vnit.ac.in

systems is revealed through signatures like the exact periodicity of entanglement dynamics and time evolution of the Floquet operator and degenerated spectra or the level crossing [76,77,79,93–96].

In a very recent work [73], we introduced a many-body Floquet spin model with an infinite-range Ising interaction. We showed that it exhibits quantum integrability. In Ref. [73], we analytically calculated the eigensystem, reduced density matrix, time evolution of the unitary operator, and entanglement dynamics for 5 to 11 qubits. We measured the entanglement dynamics using linear entropy and concurrence. For the general case $N > 11$ qubits, we resorted to numerical methods due to the complexity and fairly large calculation, as analytical solutions pose mathematical challenges. The Hamiltonian was defined as follows:

$$H(t) = \sum_{l<l'} \sigma_l^z \sigma_{l'}^z + \sum_{n=-\infty}^{\infty} \delta(n - t/\tau) \sum_{l=1}^{N} \sigma_l^y,$$

where the first term represents the Ising interaction with unit strength, while in the second term, τ is the period at which the magnetic field is applied periodically along the y axis. In various studies, the integrability in the system was identified through signatures such as the periodicity of the entanglement dynamics [94–97] and that of the Floquet operator dynamics [95] and highly degenerated spectra [79,96]. In Ref. [73] we used the same signatures to show integrability in our model for any value of N. In that study, we reported that the integrability in the system is found for a specific value of the parameter $\tau = \pi/4$, and for $\tau \neq \pi/4$ it was not. Our findings revealed that the pairwise entanglement using concurrence remains zero for various initial states, indicating the multipartite nature of the entanglement. Furthermore, the signatures of integrability show the same behavior (depending on the parity of N) for any value of N. We showed that the special case of this model is connected to the one with the nearest-neighbor Ising interaction model [94,96–100] as well as to the well-known quantum chaotic kicked top (QKT) model for specific values of parameters [101]. Once it was mapped with QKT, the integrability in the system was limited to only four qubits [102], whereas in our earlier work, we generalized it to any N using these signatures [73].

In this work, we generalize this model to include any value of the strength of Ising interaction to J. In the context of integrability, we utilize the same signatures for the same value of τ as reported in our previous work [73]. We analytically obtain the eigenvalues and eigenvectors for an even number of qubits ranging from 6 to 12. We explicitly derive the expression for entanglement measures, such as linear entropy and entanglement entropy, for various initial unentangled states. Here, we also find that these quantities exhibit a periodic nature for specific values of J other than 1 [73]. We also observe the periodic behavior of the time evolution of the unitary operator for the aforementioned cases. However, for cases involving 5, 7, 9, and 11 qubits, we numerically demonstrate the absence of these signatures. For the general case, $N > 12$, we provide sufficient numerical evidence of integrability for any even number of qubits and the absence of quantum integrability for any odd qubits by using the absence of the same signatures [73]. We also observe the decay of the maximum value of concurrence with N, indicating the increasing multipartite nature of entanglement.

The rest of this paper is organized as follows. In Sec. II, we give a brief introduction to the model investigated. In Sec. III, we give an exact analytical solution for entanglement measures such as linear entropy, entanglement entropy, and concurrence for six qubits for various initial unentangled states. In Sec. IV, the results for the analytical expression for entanglement and eigenvalues of the time-evolved unitary operator for $N = 8$, 10, and 12 qubits are presented. In Sec. V, we provide sufficient numerical evidence of the signature of quantum integrability for the general case of even $N > 12$ qubits and the absence of the quantum integrability (QI) for odd $N > 12$ qubits. In Sec. VI, a summary of the results and conclusions are given.

II. MODEL

The generalization of the Hamiltonian model from Ref. [73] is given as follows:

$$H(t) = H_I + \sum_{n=-\infty}^{\infty} \delta(n - t/\tau) H_k, \tag{1}$$

where $\delta(t)$ is a Dirac delta function and we define

$$H_I = J \sum_{l<l'} \sigma_l^z \sigma_{l'}^z, \quad H_k = \sum_{l=1}^{N} \sigma_l^y. \tag{2}$$

Here, the first term represents the Ising interaction with a field strength J, while the second term corresponds to the periodically applied magnetic field along the y axis, with a period of τ. Using Pauli matrix algebra, it can be shown easily that the two terms in Eq. (1) do not commute, i.e., $[H_I, H_k] \neq 0$. The case $J = 1$ corresponds to the Hamiltonian from Ref. [73]. The corresponding Floquet operator is given as follows:

$$\begin{aligned} \mathcal{U} &= \exp\left[-i\,\tau H_I\right] \exp\left[-i\,\tau H_k\right] \\ &= \exp\left(-i\,J\,\tau \sum_{l<l'} \sigma_l^z \sigma_{l'}^z\right) \exp\left(-i\,\tau \sum_{l=1}^{N} \sigma_l^y\right). \end{aligned} \tag{3}$$

The Ising interaction in this model is uniform and all to all. The nearest-neighbor interaction (NN) model, a special case of our model, has been extensively studied [94–100]. It exhibits permutation symmetry under the exchange of spins. Due to the presence of symmetries in the model, its effective Hilbert dimension reduces from 2^N to $N + 1$. Scrambling in models similar to ours was extensively explored in Refs. [103–108]. In Ref. [73], we showed that the model exhibits signatures of quantum integrability for the parameters $\tau = \pi/4$ and $J = 1$. The main objective of this work is to find the values of parameters at which the model shows quantum integrability. From that perspective, we restricted ourselves to the same τ while varying the field strength J. We find that the model shows identical signatures for the parameter $J = 1/2$. The Floquet operator corresponding to Eq. (1) with $\tau = \pi/4$ and $J = 1/2$ is given as follows:

$$\mathcal{U} = \exp\left(-i\frac{\pi}{8} \sum_{l<l'} \sigma_l^z \sigma_{l'}^z\right) \exp\left(-i\frac{\pi}{4} \sum_{l=1}^{N} \sigma_l^y\right). \tag{4}$$

Throughout this paper, we consistently employ the parameter values $J = 1/2$ and $\tau = \pi/4$ unless otherwise stated. In our earlier study [73], we reported that this model has a close connection to the very well known QKT model [101,109,110] and shows quantum integrability up to four qubits. In Refs. [102,110], this model was extensively studied for a smaller number of qubits ($N = 2$, 3, and 4) for these parameters. Its Hamiltonian is given by

$$H_{\rm QKT}(t) = \frac{p}{\tau'}\tilde{J}_y + \frac{k}{2j}\tilde{J}_z^2 \sum_{n=-\infty}^{\infty} \delta(t - n\tau'). \tag{5}$$

The Floquet operator in Eq. (4) also has a connection to this model for the parameters $p = \pi/2, k = j\pi/2\,(= N\pi/4)$, and $\tau' = 1$ and using many-qubit transformation $\tilde{J}_{x,y,z} = \sum_{l=1}^{2j} \sigma_l^{x,y,z}/2$, where $\sigma_l^{x,y,z}$ are the standard Pauli matrices. After this transformation Eqs. (4) and (5) are related by $\exp(-i H_{\rm QKT}) = \exp(-i NJ\tau) \times \mathcal{U}$. The overall phase (global phase) $\exp(-i NJ\tau) = \exp(-i N\pi/8)$ for $J = 1/2$ and $\tau = \pi/4$ does not alter the entanglement dynamics. However, the effect of this phase can be observed on the time period of operator dynamics when it is periodic.

In this work, we will study the time evolution from the initial states, which are localized in spherical phase space. They lie on the unit sphere with spherical coordinates (θ_0, ϕ_0). These states are the standard SU(2) coherent states and are given as follows [111,112]:

$$|\theta_0, \phi_0\rangle = \otimes^N [\cos(\theta_0/2)|0\rangle + e^{-i\phi_0} \sin(\theta_0/2)|1\rangle]. \tag{6}$$

The entanglement dynamics as a function of time can be studied by evolving these initial states using the Floquet operator $\mathcal{U}$. Our study utilizes various measures such as linear entropy [113], von Neumann entropy [114,115], and concurrence [116,117] to quantify the entanglement in the system. The commutation relation $[\mathcal{U}, \otimes_{l=1}^N \sigma_l^y] = 0$ implies that the system possesses a symmetry which is an up-down or parity symmetry (see the Supplemental Material of Ref. [73] for a detailed proof of the commutation relation). In this work, we utilize the same general basis as in Ref. [73] to solve the system analytically for any N number of qubits. The basis when N is odd is given as follows:

$$|\phi_q^{\pm}\rangle = \frac{1}{\sqrt{2}}\left(|w_q\rangle \pm i^{(N-2q)}|\overline{w_q}\rangle\right), \quad 0 \leqslant q \leqslant \frac{2j-1}{2}, \tag{7}$$

whereas for even N it is

$$|\phi_r^{\pm}\rangle = \frac{1}{\sqrt{2}}[|w_r\rangle \pm (-1)^{(j-r)}|\overline{w_r}\rangle], \quad 0 \leqslant r \leqslant j-1,$$
$$|\phi_j^{+}\rangle = \left[1/\sqrt{\binom{N}{j}}\right] \sum_{\mathcal{P}} (\otimes^j |0\rangle \otimes^j |1\rangle)_{\mathcal{P}}, \tag{8}$$

where $|w_q\rangle = [1/\sqrt{\binom{N}{q}}] \sum_{\mathcal{P}} (\otimes^q |1\rangle \otimes^{(N-q)} |0\rangle)_{\mathcal{P}}$ and $|\overline{w_q}\rangle = [1/\sqrt{\binom{N}{q}}] \sum_{\mathcal{P}} (\otimes^q |0\rangle \otimes^{(N-q)} |1\rangle)_{\mathcal{P}}$, both of which are definite particle states [118]. The $\sum_{\mathcal{P}}$ denotes the sum over all possible permutations. These basis states $|\phi_j^{\pm}\rangle$ are the eigenstates of parity operators having eigenvalues ± 1, i.e., $\otimes_{l=1}^N \sigma_l^y |\phi_j^{\pm}\rangle = \pm|\phi_j^{\pm}\rangle$. In this permutation symmetric basis, $\mathcal{U}$ is block diagonalized in two blocks, $\mathcal{U}^+$ and $\mathcal{U}^-$. Due to block diagonalization, it becomes easy to compute its nth power, which can simplify further analysis. We analytically calculate the entanglement dynamics for the coherent states $|\theta_0 = 0, \phi_0 = 0\rangle$ and $|\theta_0 = \pi/2, \phi_0 = -\pi/2\rangle$. These states have special importance when the classical phase space of the QKT model is considered [102].

III. EXACT SOLUTION FOR SIX QUBITS

By using Eq. (8) for $N = 6$, the permutation symmetric basis in which $\mathcal{U}$ is block diagonal are given as follows:

$$|\phi_0^{\pm}\rangle = \frac{1}{\sqrt{2}}(|w_0\rangle \mp |\overline{w_0}\rangle), \tag{9}$$
$$|\phi_1^{\pm}\rangle = \frac{1}{\sqrt{2}}(|w_1\rangle \pm |\overline{w_1}\rangle), \tag{10}$$
$$|\phi_2^{\pm}\rangle = \frac{1}{\sqrt{2}}(|w_2\rangle \mp |\overline{w_2}\rangle), \tag{11}$$
$$|\phi_3^{+}\rangle = \frac{1}{\sqrt{20}} \sum_{\mathcal{P}} |000111\rangle, \tag{12}$$

where $|w_0\rangle = |000000\rangle$, $|\overline{w_0}\rangle = |111111\rangle$, $|w_1\rangle = \frac{1}{\sqrt{6}}\sum_{\mathcal{P}}|000001\rangle_{\mathcal{P}}$, $|\overline{w_1}\rangle = \frac{1}{\sqrt{6}}\sum_{\mathcal{P}}|011111\rangle_{\mathcal{P}}$, $|w_2\rangle = \frac{1}{\sqrt{15}}\sum_{\mathcal{P}}|000011\rangle_{\mathcal{P}}$, and $|\overline{w_2}\rangle = \frac{1}{\sqrt{15}}\sum_{\mathcal{P}}|001111\rangle_{\mathcal{P}}$. The seven-dimensional $(N+1)$ space splits into a $4 \oplus 3$ subspace whose operators are $\mathcal{U}_{\pm}$. The unitary operator is given by

$$\mathcal{U} = \begin{pmatrix} \mathcal{U}_+ & 0_A \\ 0_B & \mathcal{U}_- \end{pmatrix}, \tag{13}$$

where $\mathcal{U}_+$ and $\mathcal{U}_-$ are (4×4) and (3×3)-dimensional matrices and 0_A and 0_B are null matrices of dimensions 4×3 and 3×4, respectively. The $\mathcal{U}_+$ and $\mathcal{U}_-$ are written in the positive and negative parity subspaces $\{\phi_0^+, \phi_1^+, \phi_2^+, \phi_3^+\}$ and $\{\phi_0^-, \phi_1^-, \phi_2^-\}$, respectively, and are obtained as follows:

$$\mathcal{U}_+ = \frac{-e^{\frac{i\pi}{8}}}{2\sqrt{2}} \begin{pmatrix} 0 & \sqrt{3} & 0 & \sqrt{5} \\ \sqrt{3}\,e^{\frac{i\pi}{4}} & 0 & \sqrt{5}\,e^{\frac{i\pi}{4}} & 0 \\ 0 & \sqrt{5} & 0 & -\sqrt{3} \\ -\sqrt{5}\,e^{\frac{i\pi}{4}} & 0 & \sqrt{3}\,e^{\frac{i\pi}{4}} & 0 \end{pmatrix}, \tag{14}$$

$$\mathcal{U}_- = \frac{e^{\frac{i\pi}{8}}}{4} \begin{pmatrix} 1 & 0 & \sqrt{15} \\ 0 & 4\,e^{\frac{i\pi}{4}} & 0 \\ \sqrt{15} & 0 & -1 \end{pmatrix}. \tag{15}$$

The eigenvalues of $\mathcal{U}_+$ and $\mathcal{U}_-$ are $\{-1, -1, 1, 1\}$ and $\{-(-1)^{1/4}, -(-1)^{3/4}, (-1)^{1/4}\}$, and the eigenvectors are $\{[\sqrt{\frac{3}{5}}, \sqrt{\frac{3}{5}}, \frac{(-1)^{3/8}}{2}\sqrt{\frac{5}{2}}, -\frac{(-1)^{3/8}}{2}\sqrt{\frac{5}{2}}]^T$, $[-2(-1)^{1/8}\sqrt{\frac{2}{5}}, 2(-1)^{1/8}\sqrt{\frac{2}{5}}, 0, 0]^T$, $[1, 1, -\frac{(-1)^{3/8}}{2}\sqrt{\frac{3}{2}}, \frac{(-1)^{3/8}}{2}\sqrt{\frac{3}{2}}]^T$, $[0, 0, 1, 1]^T\}$ and $\{[-\sqrt{\frac{3}{5}}, \sqrt{\frac{5}{3}}, 0]^T, [0, 0, 1]^T, [1, 1, 0]^T\}$, respectively. Thus, the nth time evolution of the

blocks $\mathcal{U}_{\pm}$ is given as follows:

$$\mathcal{U}_{+}^{n} = \frac{e^{\frac{in\pi}{4}}}{16}\begin{bmatrix} a_n(3+5e^{\frac{in\pi}{2}}) & 2\sqrt{6}\,b_n e^{\frac{7i\pi}{8}} & 4i\sqrt{15}\,e^{\frac{3in\pi}{4}}\sin\left(\frac{n\pi}{4}\right)\cos\left(\frac{n\pi}{2}\right) & 2\sqrt{10}\,b_n\,e^{(\frac{in\pi}{2}+\frac{3i\pi}{8})} \\ -2\sqrt{6}\,b_n\,e^{\frac{i\pi}{8}} & 8a_n & -2\sqrt{10}\,b_n\,e^{\frac{i\pi}{8}} & 0 \\ 4i\sqrt{15}\,e^{\frac{3in\pi}{4}}\sin\left(\frac{n\pi}{4}\right)\cos\left(\frac{n\pi}{2}\right) & 2\sqrt{10}\,b_n e^{\frac{7i\pi}{8}} & a_n(5+3e^{\frac{in\pi}{2}}) & -2\sqrt{6}\,b_n\,e^{(\frac{in\pi}{2}+\frac{3i\pi}{8})} \\ -2\sqrt{10}\,b_n\,e^{(\frac{in\pi}{2}+\frac{5i\pi}{8})} & 0 & 2\sqrt{6}\,b_n\,e^{(\frac{in\pi}{2}+\frac{i\pi}{8})} & 8a_n\,e^{\frac{in\pi}{2}} \end{bmatrix} \tag{16}$$

and

$$\mathcal{U}_{-}^{n} = \frac{e^{\frac{in\pi}{8}}}{8}\begin{bmatrix} 5+3\,e^{in\pi} & 0 & \sqrt{15}(1-e^{in\pi}) \\ 0 & 8\,e^{\frac{in\pi}{4}} & 0 \\ \sqrt{15}(1-e^{in\pi}) & 0 & 3+5\,e^{in\pi} \end{bmatrix}, \tag{17}$$

where $a_n = 1+e^{in\pi}$ and $b_n = 1-e^{in\pi}$. From Eqs. (16) and (17), we can observe the periodic nature of $\mathcal{U}_{+}^{n}$ ($\mathcal{U}_{-}^{n}$) with period 8 (16). Hence, the unitary operator shows periodicity with period 16, i.e., $\mathcal{U}^{n} = \mathcal{U}^{n+16}$. In Refs. [73,95] it was found that when the Hamiltonian is integrable, the corresponding unitary operator shows a periodic nature. Now, it is straightforward to perform the time evolution of any initial state and, consequently, study various quantum correlations. We further conduct a detailed analysis of two states, $|0,0\rangle$ and $|\pi/2,-\pi/2\rangle$, deriving exact expressions for the linear entropy, von Neumann entropy of a single-qubit reduced density matrix (RDM), and the concurrence between any two qubits.

A. Initial state $|000000\rangle = |\theta_0 = 0, \phi_0 = 0\rangle$

Let us first start with the state $|000000\rangle$. The nth time evolution of the unitary operator in this state is given by

$$\begin{aligned} |\psi_n\rangle &= \mathcal{U}^{n}|000000\rangle = \mathcal{U}^{n}|w_0\rangle = \mathcal{U}^{n}(|\phi_0^{+}\rangle + |\phi_0^{-}\rangle)/\sqrt{2} = (\mathcal{U}_{+}^{n}|\phi_0^{+}\rangle + \mathcal{U}_{-}^{n}|\phi_0^{-}\rangle)/\sqrt{2} \\ &= \frac{1}{\sqrt{2}}(a_1|\phi_0^{+}\rangle + a_2|\phi_1^{+}\rangle + a_3|\phi_2^{+}\rangle + a_4|\phi_3^{+}\rangle + a_5|\phi_0^{-}\rangle + a_6|\phi_2^{-}\rangle), \end{aligned} \tag{18}$$

where $a_1 = [\frac{e^{\frac{in\pi}{4}}}{16}(3+5\,e^{\frac{in\pi}{2}})(1+e^{in\pi})]$, $a_2 = \frac{e^{\frac{i\pi}{8}+\frac{in\pi}{4}}}{4}\sqrt{\frac{3}{2}}(-1+e^{in\pi})$, $a_3 = \frac{i\sqrt{15}\,e^{in\pi}}{8}[\sin(\frac{n\pi}{4}) - \sin(\frac{3n\pi}{4})]$, $a_4 = \frac{e^{(\frac{5i\pi}{8}+\frac{3in\pi}{4})}}{4}\sqrt{\frac{5}{2}}(-1+e^{in\pi})$, $a_5 = \frac{e^{\frac{in\pi}{8}}}{8}(5+3e^{in\pi})$, and $a_6 = \sqrt{15}\,e^{\frac{in\pi}{8}}(1-e^{in\pi})/8$. From $|\psi_n\rangle$, we will obtain the single-qubit RDM [$\rho_1(n) = \mathrm{Tr}_{\neq 1}(|\psi_n\rangle\langle\psi_n|)$] and the two-qubit RDM [$\rho_{12}(n) = \mathrm{Tr}_{\neq 1,2}(|\psi_n\rangle\langle\psi_n|)$].

1. Linear entropy and entanglement entropy

Linear entropy and entanglement entropy are measures used to quantify entanglement in quantum states. To calculate these measures, we obtain the single-qubit RDM $\rho_1(n)$, which is given as follows:

$$\rho_1(n) = \frac{1}{4}\begin{pmatrix} 2+a_n & w_n \\ w_n^{*} & 2-a_n \end{pmatrix}, \tag{19}$$

where

$$a_n = \frac{1}{4}\cos\left(\frac{n\pi}{8}\right)\cos\left(\frac{n\pi}{2}\right)\left[2-4\cos\left(\frac{n\pi}{4}\right)+5\cos\left(\frac{n\pi}{2}\right)+5\cos(n\pi)\right]$$

and

$$\begin{aligned} w_n = (-1)^{1/8}\,e^{-\frac{13}{8}in\pi}(-1+e^{in\pi})\{&(5+5i)\sqrt{2}+5[-1+(-1)^{1/4}]e^{\frac{in\pi}{8}} + 5\,i[(-1+i)+\sqrt{2}]e^{\frac{9in\pi}{8}} \\ &- 2\,e^{\frac{3in\pi}{4}} - 10(-1)^{1/4}e^{in\pi} - 10\,ie^{\frac{5in\pi}{4}} - 2\,(-1)^{3/4}e^{\frac{3in\pi}{2}} + [(1+5i)-(2+3i)\sqrt{2}](e^{\frac{5in\pi}{8}} + e^{\frac{13in\pi}{8}}) \\ &+10\,e^{\frac{7in\pi}{4}} + 5\,[-i+(-1)^{3/4}]e^{\frac{17in\pi}{8}} + 10\,(-1)^{3/4}e^{\frac{in\pi}{2}} + 10\,i\,e^{\frac{9in\pi}{4}}\}/64. \end{aligned}$$

The eigenvalues of $\rho_1(n)$ are λ_n and $1-\lambda_n$, where

$$\begin{aligned} \lambda_n = \frac{1}{2} - \frac{1}{16}\Bigg\{&17 + 8(2+\sqrt{2})\cos\left(\frac{n\pi}{4}\right) + 8(2-\sqrt{2})\cos\left(\frac{3n\pi}{4}\right) + 15\left[\cos\left(\frac{n\pi}{2}\right) - \sin\left(\frac{n\pi}{2}\right)\right] \\ &-8\sqrt{2}\left[\sin\left(\frac{n\pi}{4}\right) + \sin\left(\frac{3n\pi}{4}\right)\right]\Bigg\}^{\frac{1}{2}}. \end{aligned}$$

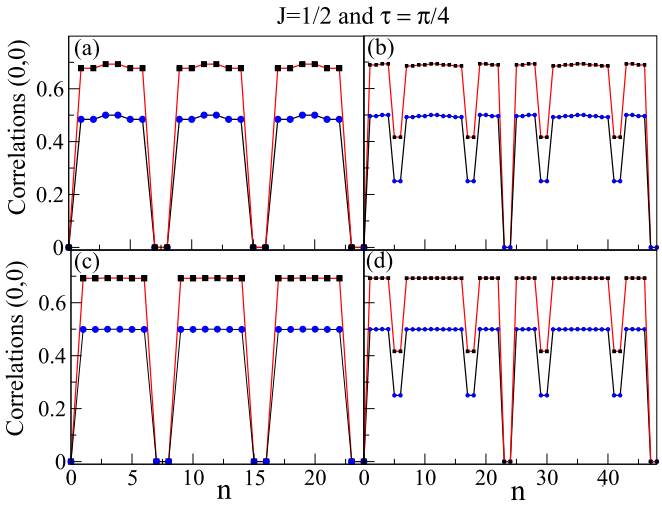

FIG. 1. Correlations (analytical values) using linear entropy (circles) and entanglement entropy (squares) are plotted for (a) 6 qubits, (b) 8 qubits, (c)10 qubits, and (d) 12 qubits for the initial state $\otimes^N|0\rangle$.

Using these eigenvalues, we can obtain the linear entropy [113] given by $2\lambda_n(1-\lambda_n)$, which is plotted in Fig. 1. The entanglement entropy [114,115] can also be calculated using $-[\lambda_n \ln\lambda_n + (1-\lambda_n)\ln(1-\lambda_n)]$ and is plotted in Fig. 1. It can be shown from the expressions and Fig. 1 that both the linear and entanglement entropy have a periodic nature with a period of 8, i.e., $S(n+8) = S(n)$. This periodic nature was previously observed in integrable systems, particularly those involving periodically kicked spin chains [73,94,96,97]. For this particular state, we provided analytical proof that the entanglement content remains unchanged for consecutive odd and even values of n (see the Supplemental Material [119] and Refs. [73,102] therein), i.e., $S^{(6)}_{(0,0)}(2n-1) = S^{(6)}_{(0,0)}(2n)$, which is shown in Fig. 1. The linear and entanglement entropy attain their maximum upper bound values of 0.5 and $\ln 2 \approx 0.6932$ for the parameters $\tau = \pi/4$ and $J = 1/2$, which was also observed in the previous study on this model [73] with the same τ but $J = 1$. We can observe from Fig. 1 that the entanglement content takes more time ($n = 3$) to reach the maximum upper bound value compared to the previous work ($n = 1$) in Ref. [73].

2. Concurrence

The linear entropy measures the entanglement between a single qubit with the rest of the qubits in a pure state, while the concurrence measures the entanglement between any pair of qubits within the system (pure or mixed). Regardless of which particular qubits are chosen, the presence of permutation symmetry in the state results in only one concurrence value [116,117]. The concurrence is given by

$$\mathcal{C}(\rho_{12}) = \max(0, \sqrt{\lambda_1} - \sqrt{\lambda_2} - \sqrt{\lambda_3} - \sqrt{\lambda_4}), \tag{20}$$

where λ_l are eigenvalues in decreasing order of $(\sigma_y \otimes \sigma_y)\rho_{12}(\sigma_y \otimes \sigma_y)\rho^*_{12}$, where ρ^*_{12} is complex conjugation in the standard (σ_z) basis. The two-qubit RDM ρ_{12} is given as follows:

$$\rho_{12}(n) = \frac{1}{4}\begin{pmatrix} b_m & a_m & a_m & d^*_m \\ a^*_m & e_m & e_m & a^*_m \\ a^*_m & e_m & e_m & a^*_m \\ d_m & a_m & a_m & f_m \end{pmatrix}, \tag{21}$$

where the coefficients are

$$b_m = \frac{1}{16}\Big[22 + 6\cos\Big(\frac{n\pi}{8}\Big) + 10\cos\Big(\frac{3n\pi}{8}\Big) + 4\cos\Big(\frac{n\pi}{2}\Big) + 10\cos\Big(\frac{5n\pi}{8}\Big) + 6\cos\Big(\frac{7n\pi}{8}\Big) + 6\cos(n\pi)\Big],$$

$$f_m = \frac{1}{4}\Big[58 + 94\cos\Big(\frac{n\pi}{8}\Big) + 78\cos\Big(\frac{n\pi}{4}\Big) + 62\cos\Big(\frac{3n\pi}{8}\Big) + 56\cos\Big(\frac{n\pi}{2}\Big) + 46\cos\Big(\frac{5n\pi}{8}\Big) + 46\cos\Big(\frac{3n\pi}{4}\Big) + 26\cos(n\pi) + 46\cos\Big(\frac{7n\pi}{8}\Big)\Big]\sin^2\Big(\frac{n\pi}{16}\Big),$$

$$d_m = \frac{1}{16}\Big\{4\cos\Big(\frac{n\pi}{2}\Big) - 6\cos(n\pi) - 2i\Big[i - 4i\sin\Big(\frac{n\pi}{2}\Big) + \sin\Big(\frac{n\pi}{8}\Big) + \sin\Big(\frac{3n\pi}{8}\Big) - \sin\Big(\frac{5n\pi}{8}\Big) - \sin\Big(\frac{7n\pi}{8}\Big)\Big]\Big\},$$

$$e_m = \frac{1}{8}\Big[3\sin\Big(\frac{n\pi}{4}\Big) + \sin\Big(\frac{3n\pi}{4}\Big)\Big]^2,$$

$$a_m = (-1)^{3/8}e^{-\frac{13}{8}in\pi}(-1+e^{in\pi})\Big[6\sqrt{2} + e^{\frac{in\pi}{8}}((2-2i) - 3\sqrt{2} + 6i\sqrt{2}e^{\frac{3in\pi}{8}} + 4(-2+\sqrt{4-3i})\cos\Big(\frac{n\pi}{2}\Big) - (4-4i)(e^{\frac{5in\pi}{8}} - e^{\frac{-3in\pi}{8}}) + (4-6e^{\frac{i\pi}{4}})e^{in\pi} - 6\sqrt{2}e^{\frac{7in\pi}{8}} - (4+4i)(e^{\frac{9in\pi}{8}} - e^{\frac{in\pi}{8}}) + 2i\sqrt{2} e^{\frac{-5in\pi}{8}} + i(-2+2i) - 3i\sqrt{2})\Big]/64\sqrt{2}.$$

By evaluating the eigenvalues of $(\sigma_y \otimes \sigma_y)\rho_{12}(\sigma_y \otimes \sigma_y)\rho^*_{12}$, we obtain fairly long expressions (please see the Supplemental Material [119] for their numerical values and also Refs. [114,116,117] therein). Using these values in Eq. (20), the computed concurrence values are plotted in Fig. 2. Similarly, concurrence is also periodic in nature, and it remains the same for consecutive odd and even values of n [119], which can be seen in Fig. 2, whereas in Ref. [73] the pairwise concurrence remained zero for all values of n. Thus, all the entanglement measure quantities are periodic in nature, which is the signature of quantum integrability [73,94–97].

B. Initial state $|++++++\rangle = |\theta_0 = \pi/2, \phi_0 = -\pi/2\rangle$

Let us now focus on another state, $|++++++\rangle_y$, where $|+\rangle_y = \frac{1}{\sqrt{2}}(|0\rangle + i|1\rangle)$ is an eigenstate of σ_y with an eigenvalue of $+1$. The evolution of this state is entirely confined to the positive parity subspace of the seven-dimensional permutation symmetric space of six-qubit Hilbert space. It can

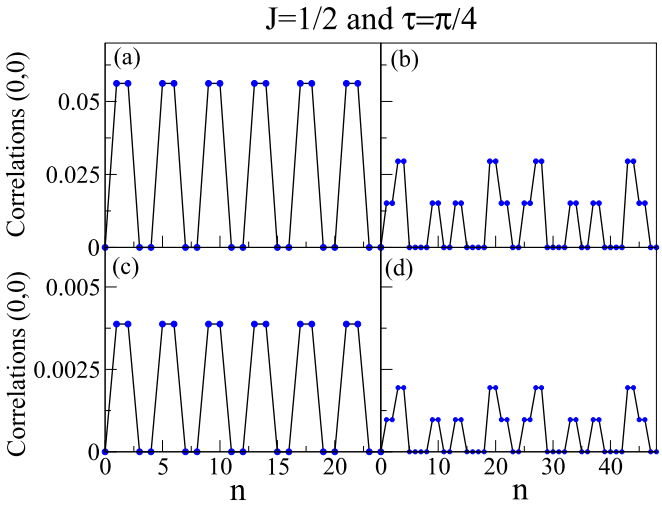

FIG. 2. The concurrence (circles) is plotted for (a) 6 qubits, (b) 8 qubits, (c) 10 qubits, and (d) 12 qubits for the initial state $\otimes^N|0\rangle$.

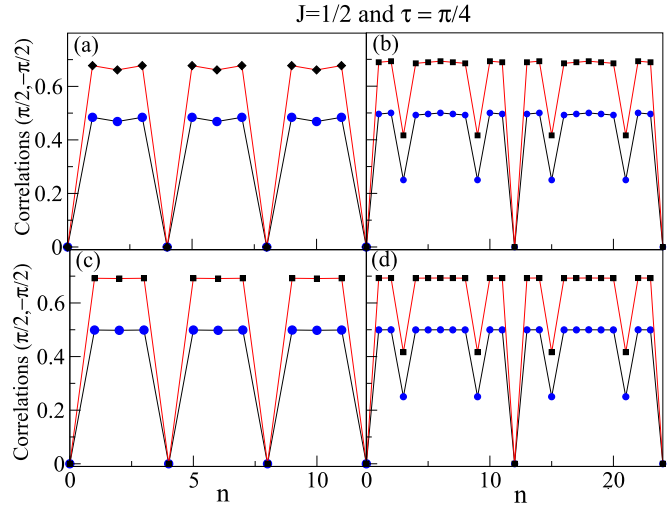

FIG. 3. Correlations using linear entropy (circles) and entanglement entropy (squares) are plotted for (a) 6 qubits, (b) 8 qubits, (c) 10 qubits, and (d) 12 qubits for the initial state $\otimes^N|+\rangle_y$.

be expressed as

$$\otimes^6|+\rangle_y = \frac{1}{4\sqrt{2}}|\phi_0^+\rangle + \frac{i\sqrt{3}}{4}|\phi_1^+\rangle - \frac{\sqrt{15}}{4\sqrt{2}}|\phi_2^+\rangle - \frac{i\sqrt{5}}{4}|\phi_3^+\rangle. \tag{22}$$

The state $|\psi_n\rangle$ can then be obtained by applying n iterations of unitary operator $\mathcal{U}$ to it as follows:

$$\begin{aligned}|\psi_n\rangle &= \mathcal{U}_+^n|++++++\rangle \\ &= e^{\frac{in\pi}{4}}(\alpha_n'|\phi_0^+\rangle + \beta_n'|\phi_1^+\rangle + \gamma_n'|\phi_2^+\rangle + \zeta_n|\phi_3^+\rangle),\end{aligned} \tag{23}$$

where the coefficients can be expressed as

$$\begin{aligned}\alpha_n' &= \frac{e^{-\frac{3}{4}in\pi}}{16\sqrt{2}}[3(-1+e^{\frac{3i\pi}{8}})+5(1+e^{\frac{7i\pi}{8}})e^{\frac{in\pi}{2}} \\ &\quad -3(1+e^{\frac{3i\pi}{8}})e^{in\pi} - 5(-1+e^{\frac{7i\pi}{8}})e^{\frac{3in\pi}{2}}], \\ \beta_n' &= \frac{\sqrt{3}\,e^{-\frac{3}{4}in\pi}}{8}[i - e^{\frac{i\pi}{8}} + (i+e^{\frac{i\pi}{8}})e^{in\pi}], \\ \gamma_n' &= \frac{i\,e^{-\frac{3}{4}in\pi}}{16}\sqrt{\frac{15}{2}}[1 - e^{\frac{3i\pi}{8}} + (i+e^{\frac{3i\pi}{8}})e^{\frac{in\pi}{2}}] \\ &\quad \times[i + (1+i)e^{\frac{in\pi}{2}} + e^{in\pi}], \\ \zeta_n &= \frac{\sqrt{5}\,e^{-\frac{1}{4}in\pi}}{8}[-i + e^{\frac{5i\pi}{8}} - (i+e^{\frac{5i\pi}{8}})e^{in\pi}].\end{aligned}$$

1. Linear and entanglement entropy

The $\rho_1(n)$ is given as follows:

$$\rho_1(n) = \frac{1}{2}\begin{bmatrix}1 & Z_n \\ Z_n^* & 1\end{bmatrix}, \tag{24}$$

where $Z_n = -i\{3[1+\cos(n\pi)] + \sqrt{2}[1-\cos(n\pi)] + 10\cos(\frac{n\pi}{2})\}/16$. The eigenvalues of $\rho_1(n)$ are λ_n and $1-\lambda_n$, where $\lambda_n = [8 - \sqrt{18+30\cos(\frac{n\pi}{2})+16\cos(n\pi)}]/16$. The linear entropy and entanglement entropy can be calculated by using eigenvalues λ_n and are plotted in Fig. 3. The entanglement content is periodic in nature with a period of 4.

2. Concurrence

The $\rho_{12}(n)$ for this state is given as follows:

$$\rho_{12}(n) = \frac{1}{2}\begin{pmatrix}h_1 & h_4 & h_4 & h_2 \\ h_4^* & h_3 & h_3 & h_6 \\ h_4^* & h_3 & h_3 & h_6 \\ h_2^* & h_6^* & h_6^* & h_1\end{pmatrix}, \tag{25}$$

where the coefficients are

$$\begin{aligned}h_1 &= \frac{1}{8}\left\{5 - \left[\cos\left(\frac{n\pi}{2}\right) + \sin\left(\frac{n\pi}{2}\right)\right]\right\}, \\ h_2 &= \frac{-1}{8}\left[1 + 3\cos\left(\frac{n\pi}{2}\right) - \sin\left(\frac{n\pi}{2}\right)\right], \\ h_3 &= \frac{1}{8}\left[3 + \cos\left(\frac{n\pi}{2}\right) + \sin\left(\frac{n\pi}{2}\right)\right], \\ h_6 &= \frac{(1-i)}{64}\left\{3(1-i)[1+\cos(n\pi)] + 2\sqrt{2}[1-\cos(n\pi)]\right. \\ &\quad \left. +10(1-i)\cos\left(\frac{n\pi}{2}\right)\right\}, \\ h_4 &= \frac{-(1+i)}{64}\left\{3(1+i)[1+\cos(n\pi)] + 2\sqrt{2}[1-\cos(n\pi)]\right. \\ &\quad \left. +10(1+i)\cos\left(\frac{n\pi}{2}\right)\right\}.\end{aligned}$$

The eigenvalues of $(\sigma_y\otimes\sigma_y)\rho_{12}(\sigma_y\otimes\sigma_y)\rho_{12}^*$ are $\{\frac{1}{4}\sin^4(\frac{n\pi}{4}), \frac{1}{256}[23 - 6\cos(\frac{n\pi}{2}) - 17\cos(n\pi) \pm 4\{\cos^2(\frac{n\pi}{2})[-5+\cos(n\pi)][(-41+16\sqrt{2})\cos(n\pi) - 109 + 16\sqrt{2} + 2(-69+16\sqrt{2})\cos(\frac{n\pi}{2})]\sin^4(\frac{n\pi}{4})\}^{\frac{1}{2}}], 0\}$. The computed concurrence values are plotted in Fig. 4. It can be observed that it is periodic in nature with a period of 4, whereas in Ref. [73] the pairwise concurrence remains zero. The periodic nature of entanglement dynamics and operator dynamics is

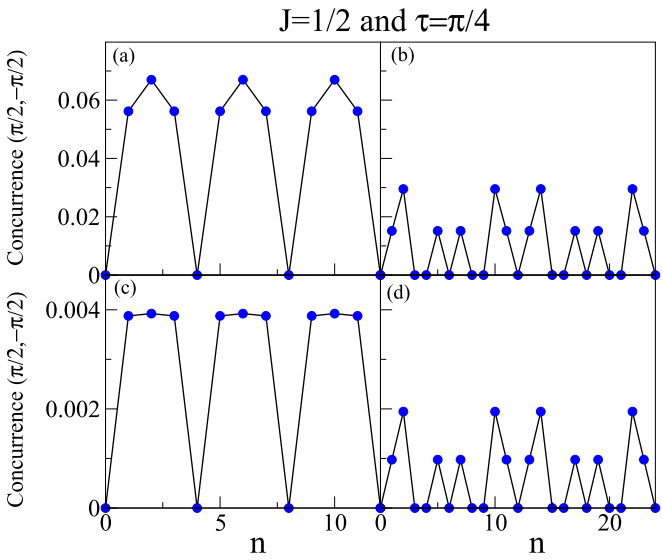

FIG. 4. The concurrence (circles) is plotted for (a) 6 qubits, (b) 8 qubits, (c) 10 qubits, and (d) 12 qubits for the initial state $\otimes^N|+\rangle_y$.

the signature of integrability [73]; hence, for six qubits the model is integrable for these parameters as well.

IV. EXACT SOLUTIONS FOR 8, 10, AND 12 QUBITS

We followed a process similar to that in Sec. III to solve the analytical cases involving $N=$ 8, 10, and 12 qubits at the particular values of $J = 1/2$ and $\tau = \pi/4$. We created distinct tables for states $\otimes^N|0\rangle$ (see Tables I and II) and $\otimes^N|+\rangle$ (see Table III) to show the analytical expression for the eigenvalues and linear entropy for 8, 10, and 12 qubits. Using these expressions, it can be shown that they exhibit a periodic behavior. For the initial state $\otimes^N|0\rangle$ and the cases of 6 and 10 qubits the period is 8, whereas for 8 and 12 qubits it is 24. This can be observed in Fig. 1. We observe that each correlation is the same for consecutive odd and even values of n [102]. We plot the analytically obtained concurrence in Fig. 2. From the values and Fig. 2, we observe that it shows a periodic nature. For $N = 6$ and 10 (8 and 12), we find $T = 4$ (12). The maximum values of concurrence ($C_{\max}$) for $N = 6$, 8, 10, and 12 are 0.05618622, 0.029509, 0.0038762, and 0.0019455, respectively (all values are close up to 12 decimal places). The reduction of $C_{\max}$ with N shows an increased multipartite nature of entanglement. The signatures of QI are obtained by limiting n to only positive integers. The data points in all the figures in this paper correspond to $n \in \mathcal{N}^+$.

Table III presents the analytical expressions for the eigenvalues and linear entropy for the initial state $\otimes^N|+\rangle$. Using these eigenvalues, the expression for entanglement entropy

TABLE I. The eigenvalues for the initial state $\otimes^N|0\rangle$ and various values of N.

N	Eigenvalues $\lambda(n)$
8	$\lambda(n) = \frac{1}{2} \pm \frac{1}{96}\Big\{\Big[5+7\cos\left(\frac{2n\pi}{3}\right)\Big]^2\Big[4\cos^2\left(\frac{3n\pi}{8}\right)+8\cos\left(\frac{3n\pi}{8}\right)\cos\left(\frac{5n\pi}{8}\right)+4\cos^2\left(\frac{5n\pi}{8}\right)\Big]+\sin^2\left(\frac{n\pi}{2}\right)\Big[9\cos^2\Big[\frac{1}{8}(3+4n)\pi\Big]$ $+147\Big\{\cos^2\Big[\frac{1}{24}(9+5n)\pi\Big]+\cos^2\Big[\frac{1}{24}(9+13n)\pi\Big]\Big\}+\sin\Big[\frac{1}{24}(9+5n)\pi\Big]\Big\{-98\sqrt{3}\cos\Big[\frac{1}{24}(9+13n)\pi\Big]+49\sin\Big[\frac{1}{24}(9+5n)\pi\Big]$ $-280\sin\Big[\frac{1}{8}(3+7n)\pi\Big]\Big\}+49\sqrt{3}\sin\Big[\frac{1}{12}(9+5n)\pi\Big]+280\sqrt{3}\cos\Big[\frac{1}{24}(9+37n)\pi\Big]\sin\Big[\frac{1}{8}(3+7n)\pi\Big]+400\sin^2\Big[\frac{1}{8}(3+7n)\pi\Big]$ $-\sin\Big[\frac{1}{24}(9+13n)\pi\Big]\Big\{98\sin\Big[\frac{1}{24}(9+5n)\pi\Big]-280\sin\Big[\frac{1}{8}(3+7n)\pi\Big]-49\sin\Big[\frac{1}{24}(9+13n)\pi\Big]\Big\}-14\cos\Big[\frac{1}{24}(9+5n)\pi\Big]$ $\Big(21\cos\Big[\frac{1}{24}(9+37n)\pi\Big]+\sqrt{3}\Big\{20\sin\Big[\frac{1}{8}(3+7n)\pi\Big]+7\sin\Big[\frac{1}{24}(9+13n)\pi\Big]\Big\}\Big)-49\sqrt{3}\sin\Big[\frac{1}{12}(9+13n)\pi\Big]+\sin\Big[\frac{1}{8}(\pi+4n\pi)\Big]$ $\Big\{18\cos\Big[\frac{1}{8}(3+4n)\pi\Big]+9\sin\Big[\frac{1}{8}(\pi+4n\pi)\Big]\Big]\Big]\Big\}^{\frac{1}{2}}$.
10	$\lambda(n) = 0.5 \pm 0.5\cos(n\pi)\Big\{0.2509765625+0.426776695296637\cos\left(\frac{n\pi}{4}\right)+0.073223304703364\cos\left(\frac{3n\pi}{4}\right)-$ $0.176776695296637\Big[\sin\left(\frac{n\pi}{4}\right)+\cos\left(\frac{3n\pi}{4}\right)\Big]+0.2490234375\Big[\cos\left(\frac{n\pi}{2}\right)-\sin\left(\frac{n\pi}{2}\right)\Big]\Big\}^{\frac{1}{2}}$.
12	$\lambda(n) = 0.5 \pm \Big\{0.041748046875+0.040916791185\cos\left(\frac{n\pi}{12}\right)+0.035634186961\Big(\cos\frac{n\pi}{4}\Big)+0.06243896484375\cos\left(\frac{n\pi}{3}\right)$ $+0.026199786034\cos\left(\frac{5n\pi}{12}\right)+0.01542619052857\cos\left(\frac{7n\pi}{12}\right)+0.02081298828125\cos\left(\frac{2n\pi}{3}\right)$ $+0.0061138599142\cos\left(\frac{3n\pi}{4}\right)+0.00070918537814\cos\left(\frac{11n\pi}{12}\right)-0.0053867977527\Big[\sin\left(\frac{n\pi}{12}\right)+\sin\left(\frac{11n\pi}{12}\right)\Big]$ $-0.0147601635233\Big[\sin\left(\frac{n\pi}{4}\right)+\sin\left(\frac{3n\pi}{4}\right)\Big]-0.036049153161\Big[\sin\left(\frac{n\pi}{3}\right)+\sin\left(\frac{2n\pi}{3}\right)\Big]$ $-0.020103802903\Big[\sin\left(\frac{5n\pi}{12}\right)+\sin\left(\frac{7n\pi}{12}\right)\Big]\Big\}^{\frac{1}{2}}$.

TABLE II. The linear entropy $S(n)$ for the initial state $\otimes^N|0\rangle$ and various values of N.

N	$S(n)$
8	$S^{(8)}_{(0,0)}(n) = \frac{1}{2}\Big(1 - \frac{1}{576}\Big[5+7\cos\Big(\frac{2n\pi}{3}\Big)\Big]^2\Big[\cos\Big(\frac{3n\pi}{8}\Big)+\cos\Big(\frac{11n\pi}{8}\Big)\Big]^2+\sin^2\Big(\frac{n\pi}{2}\Big)\Big\{-(18-9\sqrt{2})\cos(n\pi)+378\sin\Big[\frac{1}{12}(3+5n)\pi\Big]$ $+560\Big[\cos\Big(\frac{2n\pi}{3}\Big)+\sqrt{3}\sin\Big(\frac{2n\pi}{3}\Big)\Big]+196\Big[\cos\Big(\frac{4n\pi}{3}\Big)-\sqrt{3}\sin\Big(\frac{4n\pi}{3}\Big)\Big]+378\sqrt{3}\sin\Big[\frac{1}{12}(9+13n)\pi\Big]+9(-90+\sqrt{2})$ $-378\sqrt{3}\sin\Big[\frac{1}{12}(9+5n)\pi\Big]+378\sin\Big[\frac{1}{12}(3+13n)\pi\Big]-792\sin\Big[\frac{1}{4}(\pi+7n\pi)\Big]\Big\}\Big)$
10	$S^{(10)}_{(0,0)}(n) = 0.37451171875-(0.21338834765)\cos\Big(\frac{n\pi}{4}\Big)-0.036611652352\cos\Big(\frac{3n\pi}{4}\Big)+0.088388347649\Big[\sin\Big(\frac{n\pi}{4}\Big)+\sin\Big(\frac{3n\pi}{4}\Big)\Big]$ $-0.12451171875\Big[\cos\Big(\frac{n\pi}{2}\Big)-\sin\Big(\frac{n\pi}{2}\Big)\Big].$
12	$S^{(12)}_{(0,0)}(n) = \frac{1}{16}\Big(8-0.1953125e^{-in\pi}(1+e^{in\pi})^2\Big[\cos\Big(\frac{3n\pi}{8}\Big)+1.1\cos\Big(\frac{25n\pi}{24}\Big)+1.1\cos\Big(\frac{41n\pi}{24}\Big)\Big]^2-0.1667096466\Big\{\cos\Big(\frac{n\pi}{8}\Big)$ $-\cos\Big(\frac{7n\pi}{8}\Big)-0.4142135623731\Big[\sin\Big(\frac{n\pi}{8}\Big)+\sin\Big(\frac{7n\pi}{8}\Big)\Big]+[1-\cos(n\pi)]\Big[-0.944591414368\cos\Big(\frac{29n\pi}{24}\Big)$ $-0.15540858564\cos\Big(\frac{13n\pi}{24}\Big)-1.180445403469\sin\Big(\frac{13n\pi}{24}\Big)+0.724810484858\sin\Big(\frac{29n\pi}{24}\Big)\Big]\Big\}^2\Big).$

can be obtained easily (not shown here). These correlations are plotted in Fig. 3. It can be seen that they show periodic behavior. For the cases with 6 and 10 (8 and 12) qubits the period is 4 (12). The values of $C_{\max}$ for $N = 6$, 8, 10. and 12 are 0.0669873, 0.0295085, 0.00392163, and 0.0019455, respectively. Thus, for this state $C_{\max}$ also decreases with N, displaying the multipartite nature of entanglement.

For this case we also study the dynamics of the Floquet operator, and we observe that it shows periodic nature with time, i.e., $\mathcal{U}^{n+T} = \mathcal{U}^n$, where $n \geqslant 1$ and T is the period. For $N = 8$, 10, and 12 qubits, the period is 48. Through analytical calculations, we determine the eigenvalues of $\mathcal{U}$ and identify degeneracy among them (see the Supplemental Material [119]).

For the cases with 5, 7, 9, and 11 qubits, due to the complexity and fairly large expressions, we restrict ourselves to numerical results instead of analytical ones. We observe that the entanglement dynamics for both initial states do not exhibit periodic behavior (checked for n up to 1000), which is shown in Figs. 5–8 (plotted for n up to 500). We also study the Floquet operator dynamics, and we observe that it does not exhibit periodic behavior for large values of n (as shown in Fig. 12 below). The periodic behavior of entanglement dynamics and Floquet operator dynamics and the degenerated spectrum are the signature of integrability (as explained in the Introduction). In the previous study [73], we showed that this model is integrable for the parameters $J = 1$ and $\tau = \pi/4$ using these signatures, whereas in this study we observe these signatures only for even N ranging from 6 to 12. Thus, for the parameters $J = 1/2$ and $\tau = \pi/4$, the model shows integrability for 6, 8, 10, and 12 qubits and the absence of integrability for odd N ranging from 5 to 11.

V. RESULTS FOR GENERAL N QUBITS.

Using our procedure, in principle, one can solve for the case of any finite N, but various expressions for the eigensystem, Floquet operator, and its nth power become more cumbersome. Therefore, for $N > 12$ we restrict ourselves to only the numerical methods. Here, we use the same signatures used to establish integrability for $N = 6$, 8, 10, and 12 qubits. Surprisingly, we find exactly the same behavior of these signatures for the stated parameters ($J = 1/2$ and $\tau = \pi/4$). Particularly, we find that the entanglement dynamics is periodic such that for the initial state $\otimes^N|0\rangle$ ($\otimes^N|+\rangle_y$) and $N = 4m + 2$ the period is 8 (4), whereas for $N = 4m + 4$ it is 24 (12), where $m \in \{0, 1, 2, \dots\}$. The results are shown in Fig. 9. We numerically find that $C_{\max}$ tends to zero as N

TABLE III. The eigenvalues and linear entropy $S(n)$ for the initial state $\otimes^N|+\rangle$ and various values of N.

N	Eigenvalues	$S(n)$
8	$\frac{1}{2} \pm \frac{1}{48}\Big\{10\cos\Big(\frac{n\pi}{4}\Big)+7\Big[\cos\Big(\frac{5n\pi}{12}\Big)+\cos\Big(\frac{11n\pi}{12}\Big)\Big]\Big\}$	$S^{(8)}_{(\pi/2,-\pi/2)}(n) = \frac{1}{2}\Big\{1-\frac{1}{144}\cos^2\Big(\frac{n\pi}{4}\Big)\Big[5+7\cos\Big(\frac{2n\pi}{3}\Big)\Big]^2\Big\}$
10	$\frac{1}{2} \pm \frac{1}{64}\Big[\sqrt{258+510\cos\Big(\frac{n\pi}{2}\Big)+256\cos(n\pi)}\Big]$	$S^{(10)}_{(\pi/2,-\pi/2)}(n) = \frac{1}{2}\Big(1-\frac{1}{4096}\Big\{17[1+\cos(n\pi)]+\sqrt{2}[1-\cos(n\pi)]$ $+30\cos\Big(\frac{n\pi}{2}\Big)\Big\}^2\Big)$
12	$\frac{1}{2} \pm \frac{1}{64}\Big[11\cos\Big(\frac{n\pi}{12}\Big)+10\cos\Big(\frac{3n\pi}{4}\Big)+11\cos\Big(\frac{17n\pi}{12}\Big)\Big]$	$S^{(12)}_{(\pi/2,-\pi/2)}(n) = \frac{1}{2}-\frac{1}{2048}\Big[11\cos\Big(\frac{n\pi}{12}\Big)+10\cos\Big(\frac{3n\pi}{4}\Big)+11\cos\Big(\frac{17n\pi}{12}\Big)\Big]^2$

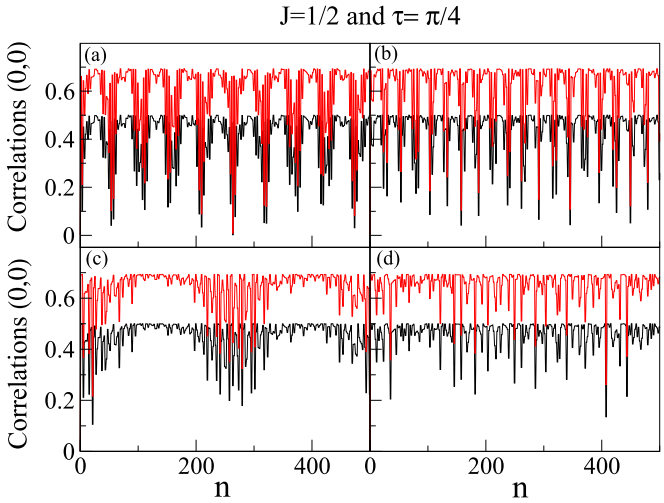

FIG. 5. Correlations using linear entropy (black) and entanglement entropy (red) are plotted for (a) 5 qubits, (b) 7 qubits, (c) 9 qubits, and (d) 11 qubits for the initial state $\otimes^N|0\rangle$.

increases for both the initial states. Thus, the entanglement becomes multipartite in nature with N. For any odd $N > 11$ with the same parameter, we find that the entanglement dynamics is not periodic at all, which is shown in Fig. 10. We observed the same nonperiodic behavior for n up to 1000 (results not shown here).

We also study the operator dynamics using a numerical method. We define $\delta(n) = \sum_{i,j}(A_{i,j}A^*_{i,j})/2N$, where $A_{i,j} = \mathcal{U}^n_{i,j} - \mathcal{U}_{i,j}$ [73]. Numerically, it is observed that the division by $2N$ ensures the average of $\delta(n)$ is 1. For any n, $\delta(n) = 0$ if and only if $\mathcal{U}^n = \mathcal{U}$, which confirms the periodic nature of $\mathcal{U}$, implying integrability. The definition above makes sure that $\delta(n)$ is invariant under the global unitary transformation (for proof see the Supplemental Material [119]). A similar definition in previous work lacked this invariance, although it did detect the periodic behavior correctly [73]. Our parameter

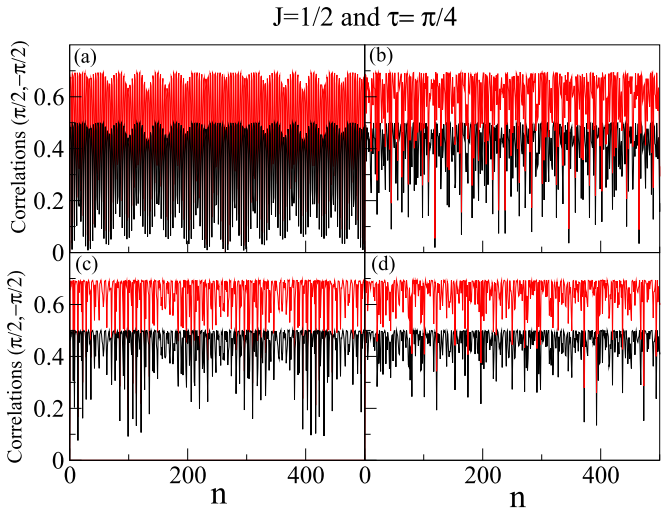

FIG. 6. Correlations using linear entropy (black) and entanglement entropy (red) are plotted for (a) 5 qubits, (b) 7 qubits, (c) 9 qubits, and (d) 11 qubits for the initial state $\otimes^N|+\rangle_y$.

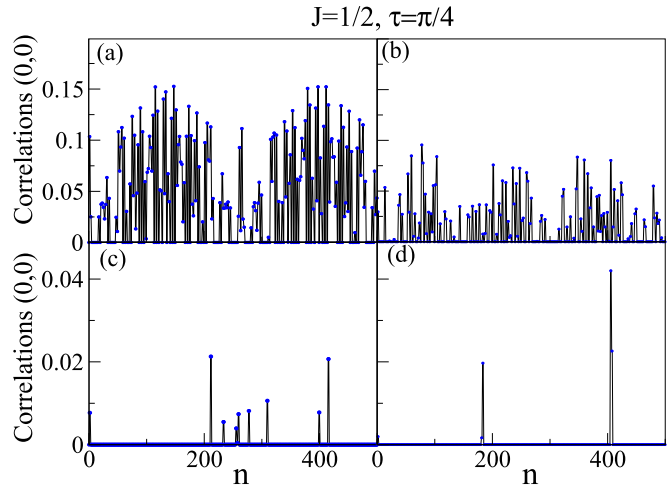

FIG. 7. The concurrence (circles) is plotted for (a) 5 qubits, (b) 7 qubits, (c) 9 qubits, and (d) 11 qubits for the initial state $\otimes^N|0\rangle$.

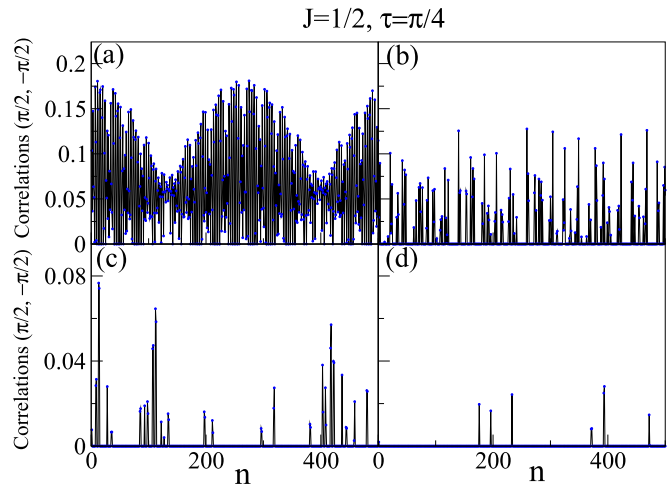

FIG. 8. The concurrence (circles) is plotted for (a) 5 qubit s, (b) 7 qubits, (c) 9 qubits, and (d) 11 qubits for the initial state $\otimes^N|+\rangle_y$.

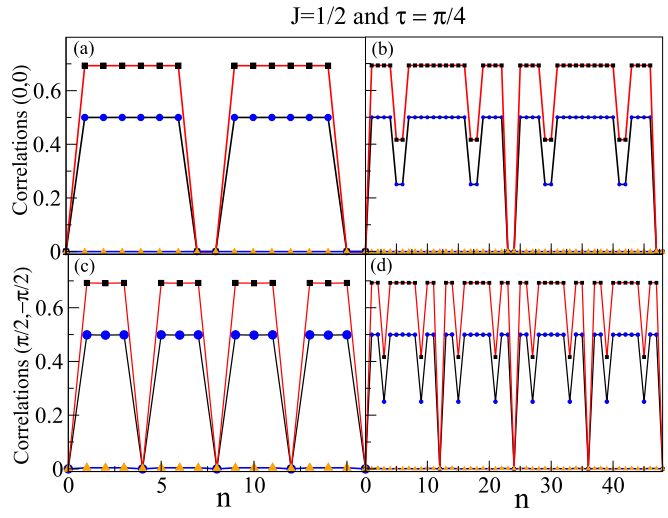

FIG. 9. Correlations using linear entropy (circles), and entanglement entropy (squares) and concurrence (triangles) are plotted for (a) 1002 qubits and (b) 1000 qubits for the initial state $\otimes^N|0\rangle$ and (c) 1002 qubits and (d) 1000 qubits for the initial state $\otimes^N|+\rangle_y$.

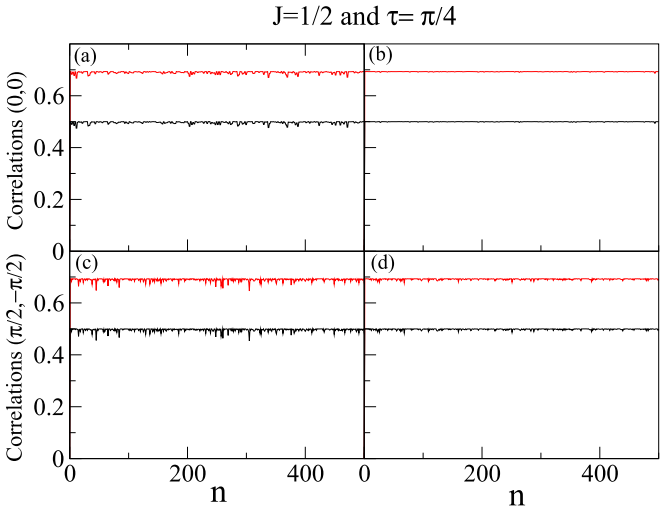

FIG. 10. Correlations using linear entropy (black) and entanglement entropy (red) are plotted for (a) 101 qubits and (b) 203 qubits for the initial state $\otimes^N|0\rangle$ and (c) 101 qubits and (d) 203 qubits for the initial state $\otimes^N|+\rangle_y$.

results are plotted in Fig. 11. We have checked periodicity for N as large as 1000 and n up to 10000 (results are not shown here). The observed period is 48 for all even $N > 6$. The same periodic nature could not be observed for (1) even N and $J \notin \{1, 1/2\}$ and (2) odd N and $J \neq 1$, which is shown in Figs. 11 and 12 (results for odd N are shown in Fig. 12). An additional signature of integrability can be found with the eigenangle spectrum of $\mathcal{U}$ [76,79,96]. We find that it is highly degenerate to take values from the finite set $\{0, \pm\pi/4, \pm\pi/8, \pm 3\pi/4, \pm 3\pi/8, \pm 5\pi/8, \pm 7\pi/8\}$ [see Fig. 13(a)], whereas for odd N, $J = 1/2$, and $\tau = \pi/4$, we find that degeneracy disappears [see Fig. 13(b)]. In fact, we find that the eigenangles are almost uniformly distributed (see Fig. 14). Thus, with these signatures, we can readily

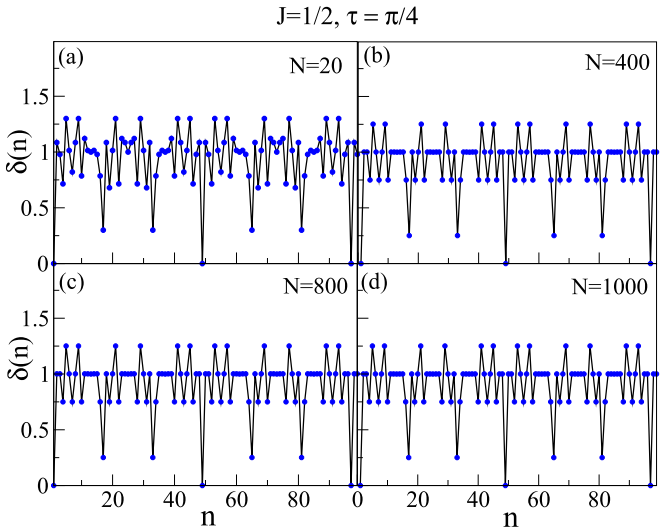

FIG. 11. The deviation $\delta(n)$ for various values of N in the integrable case.

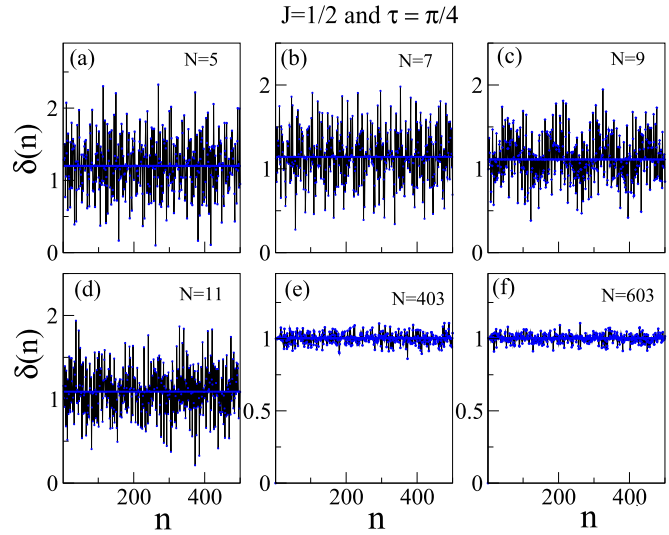

FIG. 12. The deviation $\delta(n)$ for various values of N in the nonintegrable case.

conjecture that the system is quantum integrable for any even $N > 12$, whereas for an odd N, it is not.

VI. CONCLUSIONS

In this paper, we generalized the recently introduced many-body model [73]. The model consists of qubits with all-to-all Ising interaction. Keeping the other parameters same, we generalized this interaction to J, with $J = 1$ reducing to the recent case [73]. We studied QI in the generalized version. We found that in addition to $J = 1$, QI also exists for $J = 1/2$ and *only* for an even number of qubits. We analytically calculated the eigensystem, time evolution of the unitary operator, reduced density matrix, and entanglement dynamics for an even number of qubits ranging from 6 to 12. We used linear entropy, von Neumann entropy, and concurrence to measure the entanglement dynamics for various initial unentangled states. The behavior of the entanglement dynamics and unitary

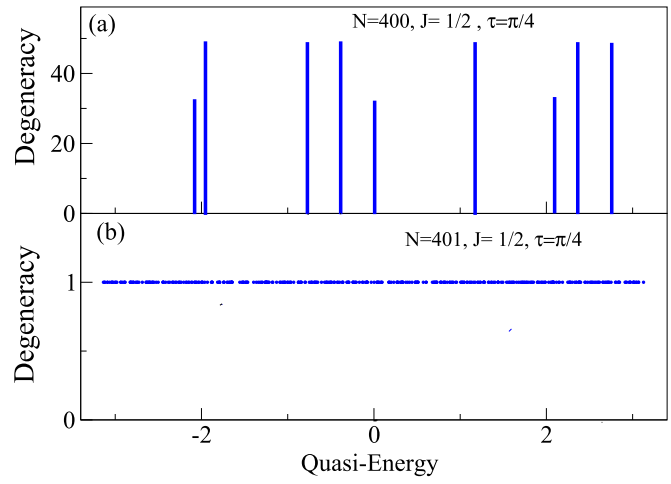

FIG. 13. Degeneracy of the quasienergies of $\mathcal{U}$ for (a) the integrable case and (b) the nonintegrable case.

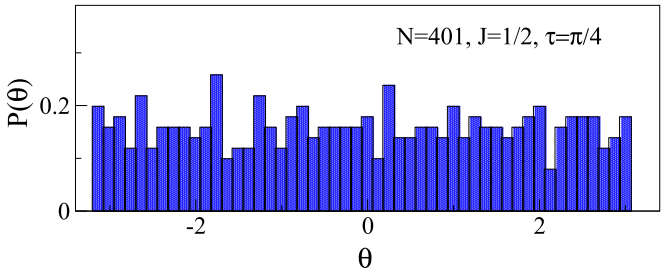

FIG. 14. Probability distribution of quasienergies.

operator dynamics is in accordance with QI systems with Ising interaction. Due to the fairly large expressions and complexity, we restricted ourselves to numerical simulations for any $N > 12$ qubits. We introduced a quantity, $\delta(n)$, to investigate the periodic nature of the time-evolution operator numerically. We showed that it remains invariant under the global unitary transformation. If this quantity is zero, then it indicates the periodic nature of the unitary operator. We observed that the entanglement dynamics and Floquet operator dynamics show periodic behavior for any even N, while for any odd N, they do not. We also observed high degeneracy in the spectra for an even number of qubits. However, for odd N, the degeneracy in the spectra disappears. We observed that the pairwise concurrence tends to zero with N, indicating the multipartite nature of entanglement. Thus, we can very well conjuncture that the system also exhibits quantum integrability for parameters $J = 1/2$ and $\tau = \pi/4$ for any even number of qubits, whereas it is absent for any odd number of qubits.

In recent work, a generalization of the Hubbard-Stratonovich transformation was employed to get an exact analytical solution for quantum-strong long-range Ising chains [120]. Our model can be explored further in that direction. It should be noted that our model is disorder-free (clean) and the integrability exists only for the special values of the parameters J and τ [73]. Applying minor perturbations in either of the parameters can destroy the quantum integrability by breaking the conserved quantities so the exact solutions are no longer possible [73,121] as far as we know. This can lead to a transition from integrable to chaotic behavior of the system. Experimental verification of our model is possible, although it is challenging. In fact, a disordered version of our model was studied in detail in Ref. [121]. Experimental verification of our results (for a smaller number of qubits) could be conducted in various setups such as NMR [122], superconducting qubits [123], and laser-cooled atoms [124], where the QKT has been implemented, whereas for a large number of qubits (of the order of hundreds), one could use ion traps [15,125]. The validity of our conjecture could be established in this setup.

While our study has successfully identified integrability in this model for the specified values of parameters $J = 1, 1/2$ and $\tau = \pi/4$, we think our work raises several open questions. A few of them are as follows: (1) As the number of qubits increases, entanglement becomes multipartite in nature. One such measure is the Meyer and Wallach Q measure, which is very much related to linear entropy, and we studied it here. Further analysis using various multipartite entanglement measures would be an interesting direction to pursue [126–129]. (2) It would be interesting to determine whether there other possible values of J that exhibit integrability within this framework. (3) Our findings encourage further exploration to search for other integrable systems in which all-to-all interaction is present.

ACKNOWLEDGMENTS

The authors are grateful to the Department of Science and Technology (DST) for their generous financial support, making this research possible through sanctioned Project No. SR/FST/PSI/2017/5(C) to the Department of Physics of VNIT, Nagpur. We are also grateful to A. Purohit for his discussion of and suggestions for the manuscript. We thank the anonymous referees for their valuable comments.

[1] T. Dauxois, S. Ruffo, E. Arimondo, and M. Wilkens, *Dynamics and Thermodynamics of Systems with Long-Range Interactions: An Introduction* (Springer, Berlin, 2002).

[2] B. Sutherland, *Beautiful Models: 70 Years of Exactly Solved Quantum Many-Body Problems* (World Scientific, Singapore, 2004).

[3] A. Campa, T. Dauxois, D. Fanelli, and S. Ruffo, *Physics of Long-Range Interacting Systems* (Oxford University Press, Oxford, 2014).

[4] P. E. S. Wormer, F. Mulder, and A. V. der Avoird, Quantum theoretical calculations of van der Waals interactions between molecules. Anisotropic long range interactions, Int. J. Quantum Chem. **11**, 959 (1977).

[5] A. Salam, *Molecular Quantum Electrodynamics: Long-Range Intermolecular Interactions* (Wiley, Hoboken, NJ, 2009).

[6] A. D. Dolgov, Long-range forces in the universe, Phys. Rep. **320**, 1 (1999).

[7] A. Nusser, S. S. Gubser, and P. J. E. Peebles, Structure formation with a long-range scalar dark matter interaction, Phys. Rev. D **71**, 083505 (2005).

[8] L. G. van den Aarssen, T. Bringmann, and C. Pfrommer, Is dark matter with long-range interactions a solution to all small-scale problems of λ cold dark matter cosmology? Phys. Rev. Lett. **109**, 231301 (2012).

[9] I. Esteban and J. Salvado, Long range interactions in cosmology: Implications for neutrinos, J. Cosmol. Astropart. Phys. **2021**, 036 (2021).

[10] P. Chomaz and F. Gulminelli, Phase transitions in finite systems, in *Dynamics and Thermodynamics of Systems with Long-Range Interactions* (Springer, Berlin, 2002), pp. 68–129.

[11] Y. Elskens, *Microscopic Dynamics of Plasmas and Chaos* (CRC Press, Boca Raton, FL, 2019).

[12] J. Miller, Statistical mechanics of Euler equations in two dimensions, Phys. Rev. Lett. **65**, 2137 (1990).

[13] A. Schuckert, I. Lovas, and M. Knap, Nonlocal emergent hydrodynamics in a long-range quantum spin system, Phys. Rev. B **101**, 020416(R) (2020).

[14] A. Morningstar, N. O'Dea, and J. Richter, Hydrodynamics in long-range interacting systems with center-of-mass conservation, Phys. Rev. B **108**, L020304 (2023).

[15] N. Defenu, T. Donner, T. Macrì, G. Pagano, S. Ruffo, and A. Trombettoni, Long-range interacting quantum systems, Rev. Mod. Phys. **95**, 035002 (2023).
[16] I. Buluta and F. Nori, Quantum simulators, Science **326**, 108 (2009).
[17] I. M. Georgescu, S. Ashhab, and F. Nori, Quantum simulation, Rev. Mod. Phys. **86**, 153 (2014).
[18] C. Gross and I. Bloch, Quantum simulations with ultracold atoms in optical lattices, Science **357**, 995 (2017).
[19] X.-L. Deng, D. Porras, and J. I. Cirac, Effective spin quantum phases in systems of trapped ions, Phys. Rev. A **72**, 063407 (2005).
[20] R. Islam *et al.*, Onset of a quantum phase transition with a trapped ion quantum simulator, Nat. Commun. **2**, 377 (2011).
[21] A. Bermúdez, L. Tagliacozzo, G. Sierra, and P. Richerme, Long-range Heisenberg models in quasiperiodically driven crystals of trapped ions, Phys. Rev. B **95**, 024431 (2017).
[22] K. Baumann, C. Guerlin, F. Brennecke, and T. Esslinger, Dicke quantum phase transition with a superfluid gas in an optical cavity, Nature (London) **464**, 1301 (2010).
[23] B. Yan, S. A. Moses, B. Gadway, J. P. Covey, K. R. Hazzard, A. M. Rey, D. S. Jin, and J. Ye, Observation of dipolar spin-exchange interactions with lattice-confined polar molecules, Nature (London) **501**, 521 (2013).
[24] T. Lahaye, C. Menotti, L. Santos, M. Lewenstein, and T. Pfau, The physics of dipolar bosonic quantum gases, Rep. Prog. Phys. **72**, 126401 (2009).
[25] L. Chomaz, I. Ferrier-Barbut, F. Ferlaino, B. Laburthe-Tolra, B. L. Lev, and T. Pfau, Dipolar physics: A review of experiments with magnetic quantum gases, Rep. Prog. Phys. **86**, 026401 (2022).
[26] J. C. Smith, D. Baillie, and P. B. Blakie, Supersolidity and crystallization of a dipolar gas in an infinite tube, Phys. Rev. A **107**, 033301 (2023).
[27] M. Saffman, T. G. Walker, and K. Mølmer, Quantum information with Rydberg atoms, Rev. Mod. Phys. **82**, 2313 (2010).
[28] A. Griesmaier, J. Werner, S. Hensler, J. Stuhler, and T. Pfau, Bose-Einstein condensation of chromium, Phys. Rev. Lett. **94**, 160401 (2005).
[29] Q. Beaufils, R. Chicireanu, T. Zanon, B. Laburthe-Tolra, E. Maréchal, L. Vernac, J.-C. Keller, and O. Gorceix, All-optical production of chromium Bose-Einstein condensates, Phys. Rev. A **77**, 061601(R) (2008).
[30] S. Baier, M. J. Mark, D. Petter, K. Aikawa, L. Chomaz, Z. Cai, M. Baranov, P. Zoller, and F. Ferlaino, Extended Bose-Hubbard models with ultracold magnetic atoms, Science **352**, 201 (2016).
[31] O. Firstenberg, T. Peyronel, Q.-Y. Liang, A. V. Gorshkov, M. D. Lukin, and V. Vuletić, Attractive photons in a quantum nonlinear medium, Nature (London) **502**, 71 (2013).
[32] L. Childress, M. V. Gurudev Dutt, J. M. Taylor, A. S. Zibrov, F. Jelezko, J. Wrachtrup, P. R. Hemmer, and M. D. Lukin, Coherent dynamics of coupled electron and nuclear spin qubits in diamond, Science **314**, 281 (2006).
[33] A. Sanyal, B. R. Lajoie, G. Jain, and J. Dekker, The long-range interaction landscape of gene promoters, Nature (London) **489**, 109 (2012).
[34] A. V. Shytov, D. A. Abanin, and L. S. Levitov, Long-range interaction between adatoms in graphene, Phys. Rev. Lett. **103**, 016806 (2009).
[35] M. Kastner, Diverging equilibration times in long-range quantum spin models, Phys. Rev. Lett. **106**, 130601 (2011).
[36] Z.-X. Gong, M. F. Maghrebi, A. Hu, M. Foss-Feig, P. Richerme, C. Monroe, and A. V. Gorshkov, Kaleidoscope of quantum phases in a long-range interacting spin-1 chain, Phys. Rev. B **93**, 205115 (2016).
[37] M. Avellino, A. J. Fisher, and S. Bose, Quantum communication in spin systems with long-range interactions, Phys. Rev. A **74**, 012321 (2006).
[38] Z. Eldredge, Z.-X. Gong, J. T. Young, A. H. Moosavian, M. Foss-Feig, and A. V. Gorshkov, Fast quantum state transfer and entanglement renormalization using long-range interactions, Phys. Rev. Lett. **119**, 170503 (2017).
[39] A. Solfanelli, G. Giachetti, M. Campisi, S. Ruffo, and N. Defenu, Quantum heat engine with long-range advantages, New J. Phys. **25**, 033030 (2023).
[40] D. Lewis, A. Benhemou, N. Feinstein, L. Banchi, and S. Bose, Optimal quantum spatial search with one-dimensional long-range interactions, Phys. Rev. Lett. **126**, 240502 (2021).
[41] D. Lewis, L. Banchi, Y. H. Teoh, R. Islam, and S. Bose, Ion trap long-range XY model for quantum state transfer and optimal spatial search, Quantum Sci. Technol. **8**, 035025 (2023).
[42] L. Pezze, A. Smerzi, M. K. Oberthaler, R. Schmied, and P. Treutlein, Quantum metrology with nonclassical states of atomic ensembles, Rev. Mod. Phys. **90**, 035005 (2018).
[43] F. M. Gambetta, C. Zhang, M. Hennrich, I. Lesanovsky, and W. Li, Long-range multibody interactions and three-body antiblockade in a trapped Rydberg ion chain, Phys. Rev. Lett. **125**, 133602 (2020).
[44] P. Hauke and L. Tagliacozzo, Spread of correlations in long-range interacting quantum systems, Phys. Rev. Lett. **111**, 207202 (2013).
[45] L. Colmenarez and D. J. Luitz, Lieb-Robinson bounds and out-of-time order correlators in a long-range spin chain, Phys. Rev. Res. **2**, 043047 (2020).
[46] S. Bravyi, M. B. Hastings, and F. Verstraete, Lieb-Robinson bounds and the generation of correlations and topological quantum order, Phys. Rev. Lett. **97**, 050401 (2006).
[47] J. Zhang, G. Pagano, P. W. Hess, A. Kyprianidis, P. Becker, H. Kaplan, A. V. Gorshkov, Z.-X. Gong, and C. Monroe, Observation of a many-body dynamical phase transition with a 53-qubit quantum simulator, Nature (London) **551**, 601 (2017).
[48] P. Jurcevic, H. Shen, P. Hauke, C. Maier, T. Brydges, C. Hempel, B. P. Lanyon, M. Heyl, R. Blatt, and C. F. Roos, Direct observation of dynamical quantum phase transitions in an interacting many-body system, Phys. Rev. Lett. **119**, 080501 (2017).
[49] W. Dür, L. Hartmann, M. Hein, M. Lewenstein, and H.-J. Briegel, Entanglement in spin chains and lattices with long-range Ising-type interactions, Phys. Rev. Lett. **94**, 097203 (2005).
[50] A. Kuzmak, Entanglement and quantum state geometry of a spin system with all-range Ising-type interaction, J. Phys. A **51**, 175305 (2018).
[51] X. Deng, G. Masella, G. Pupillo, and L. Santos, Universal algebraic growth of entanglement entropy in many-body localized systems with power-law interactions, Phys. Rev. Lett. **125**, 010401 (2020).

[52] J. T. Schneider, J. Despres, S. J. Thomson, L. Tagliacozzo, and L. Sanchez-Palencia, Spreading of correlations and entanglement in the long-range transverse Ising chain, Phys. Rev. Res. **3**, L012022 (2021).

[53] J. Richter, O. Lunt, and A. Pal, Transport and entanglement growth in long-range random Clifford circuits, Phys. Rev. Res. **5**, L012031 (2023).

[54] B. Amghar, A. Slaoui, J. Elfakir, and M. Daoud, Geometrical, topological, and dynamical description of N interacting spin-s particles in a long-range Ising model and their interplay with quantum entanglement, Phys. Rev. A **107**, 032402 (2023).

[55] B. Kloss and Y. B. Lev, Spin transport in disordered long-range interacting spin chain, Phys. Rev. B **102**, 060201(R) (2020).

[56] M. Song, J. Zhao, Y. Qi, J. Rong, and Z. Y. Meng, Quantum criticality and entanglement for the two-dimensional long-range Heisenberg bilayer, Phys. Rev. B **109**, L081114 (2024).

[57] A. Duha and T. Bilitewski, Two-mode squeezing in Floquet-engineered power-law interacting spin models, Phys. Rev. A **109**, L061304 (2024).

[58] S. Pappalardi, A. Russomanno, B. Žunkovič, F. Iemini, A. Silva, and R. Fazio, Scrambling and entanglement spreading in long-range spin chains, Phys. Rev. B **98**, 134303 (2018).

[59] M. Gärttner, J. G. Bohnet, A. Safavi-Naini, M. L. Wall, J. J. Bollinger, and A. M. Rey, Measuring out-of-time-order correlations and multiple quantum spectra in a trapped-ion quantum magnet, Nat. Phys. **13**, 781 (2017).

[60] J. W. Britton, B. C. Sawyer, A. C. Keith, C.-C. J. Wang, J. K. Freericks, H. Uys, M. J. Biercuk, and J. J. Bollinger, Engineered two-dimensional Ising interactions in a trapped-ion quantum simulator with hundreds of spins, Nature (London) **484**, 489 (2012).

[61] P. Schauß, M. Cheneau, M. Endres, T. Fukuhara, S. Hild, A. Omran, T. Pohl, C. Gross, S. Kuhr, and I. Bloch, Observation of spatially ordered structures in a two-dimensional Rydberg gas, Nature (London) **491**, 87 (2012).

[62] D. Peter, S. Müller, S. Wessel, and H. P. Büchler, Anomalous behavior of spin systems with dipolar interactions, Phys. Rev. Lett. **109**, 025303 (2012).

[63] P. Jurcevic, B. P. Lanyon, P. Hauke, C. Hempel, P. Zoller, R. Blatt, and C. F. Roos, Quasiparticle engineering and entanglement propagation in a quantum many-body system, Nature (London) **511**, 202 (2014).

[64] K. R. A. Hazzard, B. Gadway, M. Foss-Feig, B. Yan, S. A. Moses, J. P. Covey, N. Y. Yao, M. D. Lukin, J. Ye, D. S. Jin, and A. M. Rey, Many-body dynamics of dipolar molecules in an optical lattice, Phys. Rev. Lett. **113**, 195302 (2014).

[65] P. Richerme, Z.-X. Gong, A. Lee, C. Senko, J. Smith, M. Foss-Feig, S. Michalakis, A. V. Gorshkov, and C. Monroe, Non-local propagation of correlations in quantum systems with long-range interactions, Nature (London) **511**, 198 (2014).

[66] J. S. Douglas, H. Habibian, C.-L. Hung, A. V. Gorshkov, H. J. Kimble, and D. E. Chang, Quantum many-body models with cold atoms coupled to photonic crystals, Nat. Photon. **9**, 326 (2015).

[67] A. de Paz, A. Sharma, A. Chotia, E. Maréchal, J. H. Huckans, P. Pedri, L. Santos, O. Gorceix, L. Vernac, and B. Laburthe-Tolra, Nonequilibrium quantum magnetism in a dipolar lattice gas, Phys. Rev. Lett. **111**, 185305 (2013).

[68] J. Marino and A. M. Rey, Cavity-QED simulator of slow and fast scrambling, Phys. Rev. A **99**, 051803(R) (2019).

[69] N. Sauerwein, F. Orsi, P. Uhrich, S. Bandyopadhyay, F. Mattiotti, T. Cantat-Moltrecht, G. Pupillo, P. Hauke, and J.-P. Brantut, Engineering random spin models with atoms in a high-finesse cavity, Nat. Phys. **19**, 1128 (2023).

[70] Z. Liu and P. Zhang, Signature of Scramblon effective field theory in random spin models, Phys. Rev. Lett. **132**, 060201 (2024).

[71] B. Žunkovič and A. Zegarra, Mean-field dynamics of an infinite-range interacting quantum system: Chaos, dynamical phase transition, and localization, Phys. Rev. B **109**, 064309 (2024).

[72] M. Kumari and Á. M. Alhambra, Eigenstate entanglement in integrable collective spin models, Quantum **6**, 701 (2022).

[73] H. Sharma and U. T. Bhosale, Exactly solvable dynamics and signatures of integrability in an infinite-range many-body Floquet spin system, Phys. Rev. B **109**, 014412 (2024).

[74] O. Babelon, D. Bernard, and M. Talon, *Introduction to Classical Integrable Systems* (Cambridge University Press, Cambridge, 2003).

[75] A. L. Retore, Introduction to classical and quantum integrability, J. Phys. A **55**, 173001 (2022).

[76] H. Owusu, K. Wagh, and E. Yuzbashyan, The link between integrability, level crossings and exact solution in quantum models, J. Phys. A **42**, 035206 (2009).

[77] A. Doikou, S. Evangelisti, G. Feverati, and N. Karaiskos, Introduction to quantum integrability, Int. J. Mod. Phys. A **25**, 3307 (2010).

[78] A. Gubin and L. F. Santos, Quantum chaos: An introduction via chains of interacting spins 1/2, Am. J. Phys. **80**, 246 (2012).

[79] E. A. Yuzbashyan and B. S. Shastry, Quantum integrability in systems with finite number of levels, J. Stat. Phys. **150**, 704 (2013).

[80] T. Gombor and B. Pozsgay, Integrable spin chains and cellular automata with medium-range interaction, Phys. Rev. E **104**, 054123 (2021).

[81] E. Vernier, H.-C. Yeh, L. Piroli, and A. Mitra, Strong zero modes in integrable quantum circuits, Phys. Rev. Lett. **133**, 050606 (2024).

[82] M. Wadati, T. Nagao, and K. Hikami, Quantum integrable systems, Phys. D (Amsterdam, Neth.) **68**, 162 (1993).

[83] L. A. Lambe and D. E. Radford, *Introduction to the Quantum Yang-Baxter Equation and Quantum Groups: An Algebraic Approach*, Mathematics and Its Applications, Vol. 423 (Springer, 2013).

[84] R. J. Baxter, *Exactly Solved Models in Statistical Mechanics* (Elsevier, 2016).

[85] M. Gaudin, *The Bethe Wavefunction* (Cambridge University Press, Cambridge, 2014).

[86] M. Zheng, Y. Qiao, Y. Wang, J. Cao, and S. Chen, Exact solution of the Bose-Hubbard model with unidirectional hopping, Phys. Rev. Lett. **132**, 086502 (2024).

[87] H. Bethe, Zur Theorie der Metalle: I. Eigenwerte und Eigenfunktionen der linearen Atomkette, Z. Phys. **71**, 205 (1931).

[88] L. Faddeev, Algebraic aspects of the Bethe ansatz, Int. J. Mod. Phys. A **10**, 1845 (1995).

[89] F. Pan and J. P. Draayer, Analytical solutions for the LMG model, Phys. Lett. B **451**, 1 (1999).

[90] T. Bargheer, N. Beisert, and F. Loebbert, Boosting nearest-neighbour to long-range integrable spin chains, J. Stat. Mech. (2008) L11001.

[91] M. V. Berry and M. Tabor, Level clustering in the regular spectrum, Proc. R. Soc. London, Ser. A **356**, 375 (1977).

[92] U. T. Bhosale, Superposition and higher-order spacing ratios in random matrix theory with application to complex systems, Phys. Rev. B **104**, 054204 (2021).

[93] Y. Y. Atas, E. Bogomolny, O. Giraud, and G. Roux, Distribution of the ratio of consecutive level spacings in random matrix ensembles, Phys. Rev. Lett. **110**, 084101 (2013).

[94] S. K. Mishra, A. Lakshminarayan, and V. Subrahmanyam, Protocol using kicked Ising dynamics for generating states with maximal multipartite entanglement, Phys. Rev. A **91**, 022318 (2015).

[95] R. Pal and A. Lakshminarayan, Entangling power of time-evolution operators in integrable and nonintegrable many-body systems, Phys. Rev. B **98**, 174304 (2018).

[96] G. K. Naik, R. Singh, and S. K. Mishra, Controlled generation of genuine multipartite entanglement in Floquet Ising spin models, Phys. Rev. A **99**, 032321 (2019).

[97] A. Lakshminarayan and V. Subrahmanyam, Multipartite entanglement in a one-dimensional time-dependent Ising model, Phys. Rev. A **71**, 062334 (2005).

[98] T. J. G. Apollaro, G. M. Palma, and J. Marino, Entanglement entropy in a periodically driven quantum Ising ring, Phys. Rev. B **94**, 134304 (2016).

[99] B. Bertini, P. Kos, and T. Prosen, Entanglement spreading in a minimal model of maximal many-body quantum chaos, Phys. Rev. X **9**, 021033 (2019).

[100] R. K. Shukla and S. K. Mishra, Characteristic, dynamic, and near-saturation regions of out-of-time-order correlation in Floquet Ising models, Phys. Rev. A **106**, 022403 (2022).

[101] F. Haake, M. Kuś, and R. Scharf, Classical and quantum chaos for a kicked top, Z. Phys. B **65**, 381 (1987).

[102] S. Dogra, V. Madhok, and A. Lakshminarayan, Quantum signatures of chaos, thermalization, and tunneling in the exactly solvable few-body kicked top, Phys. Rev. E **99**, 062217 (2019).

[103] R. Belyansky, P. Bienias, Y. A. Kharkov, A. V. Gorshkov, and B. Swingle, Minimal model for fast scrambling, Phys. Rev. Lett. **125**, 130601 (2020).

[104] Z. Li, S. Choudhury, and W. V. Liu, Fast scrambling without appealing to holographic duality, Phys. Rev. Res. **2**, 043399 (2020).

[105] C. Yin and A. Lucas, Bound on quantum scrambling with all-to-all interactions, Phys. Rev. A **102**, 022402 (2020).

[106] Z. Li, S. Choudhury, and W. V. Liu, Long-range-ordered phase in a quantum Heisenberg chain with interactions beyond nearest neighbors, Phys. Rev. A **104**, 013303 (2021).

[107] S.-S. Li, R.-Z. Huang, and H. Fan, Fast scrambling dynamics and many-body localization transition in an all-to-all disordered quantum spin model, Phys. Rev. B **106**, 024309 (2022).

[108] D. Wanisch, J. D. Arias Espinoza, and S. Fritzsche, Information scrambling and the correspondence of entanglement dynamics and operator dynamics in systems with nonlocal interactions, Phys. Rev. B **107**, 205127 (2023).

[109] F. Haake, *Quantum Signatures of Chaos*, 3rd ed. (Springer, Berlin, 2010).

[110] U. T. Bhosale and M. S. Santhanam, Periodicity of quantum correlations in the quantum kicked top, Phys. Rev. E **98**, 052228 (2018).

[111] R. J. Glauber and F. Haake, Superradiant pulses and directed angular momentum states, Phys. Rev. A **13**, 357 (1976).

[112] R. R. Puri, *Mathematical Methods of Quantum Optics* (Springer, Berlin, 2001).

[113] F. Buscemi, P. Bordone, and A. Bertoni, Linear entropy as an entanglement measure in two-fermion systems, Phys. Rev. A **75**, 032301 (2007).

[114] M. A. Nielsen and I. L. Chuang, *Quantum Computation and Quantum Information* (Cambridge University Press, Cambridge, 2000).

[115] G. Benenti, G. Casati, and G. Strini, *Principles of Quantum Computation and Information: Basic Tools and Special Topics* (World Scientific, Singapore, 2004), Vol. 2.

[116] W. K. Wootters, Entanglement of formation of an arbitrary state of two qubits, Phys. Rev. Lett. **80**, 2245 (1998).

[117] W. K. Wootters, Entanglement of formation and concurrence, Quantum Inf. Comput. **1**, 27 (2001).

[118] V. S. Vijayaraghavan, U. T. Bhosale, and A. Lakshminarayan, Entanglement transitions in random definite particle states, Phys. Rev. A **84**, 032306 (2011).

[119] See Supplemental Material at http://link.aps.org/supplemental/10.1103/PhysRevB.110.064313 for detailed analysis of analytical solutions of the entanglement measures such as linear entropy, entanglement entropy, and concurrence for the cases of 6,8,10, and 12 qubits. We also show that the quantity $\delta(n)$ remains invariant under global unitary transformation.

[120] J. Román-Roche, V. Herráiz-López, and D. Zueco, Exact solution for quantum strong long-range models via a generalized Hubbard-Stratonovich transformation, Phys. Rev. B **108**, 165130 (2023).

[121] Manju C, A. Lakshminarayan, and U. Divakaran, Chaos controlled and disorder driven phase transitions by breaking permutation symmetry, arXiv:2406.00521.

[122] V. R. Krithika, V. S. Anjusha, U. T. Bhosale, and T. S. Mahesh, NMR studies of quantum chaos in a two-qubit kicked top, Phys. Rev. E **99**, 032219 (2019).

[123] C. Neill *et al.*, Ergodic dynamics and thermalization in an isolated quantum system, Nat. Phys. **12**, 1037 (2016).

[124] S. Chaudhury, A. Smith, B. E. Anderson, S. Ghose, and P. S. Jessen, Nature (London) **461**, 768 (2009).

[125] C. Monroe *et al.*, Programmable quantum simulations of spin systems with trapped ions, Rev. Mod. Phys. **93**, 025001 (2021).

[126] P. Hauke, M. Heyl, L. Tagliacozzo, and P. Zoller, Measuring multipartite entanglement through dynamic susceptibilities, Nat. Phys. **12**, 778 (2016).

[127] S. Szalay, Multipartite entanglement measures, Phys. Rev. A **92**, 042329 (2015).

[128] H. Li, T. Gao, and F. Yan, Parametrized multipartite entanglement measures, Phys. Rev. A **109**, 012213 (2024).

[129] J. L. Beckey, N. Gigena, P. J. Coles, and M. Cerezo, Computable and operationally meaningful multipartite entanglement measures, Phys. Rev. Lett. **127**, 140501 (2021).